

# Sm(Co,Cu)<sub>5</sub>/Fe exchange spring multilayer films with high energy product

J. Zhang, Y. K. Takahashi, R. Gopalan, and K. Hono

*National Institute for Material Science (NIMS), 1-2-1 Sengen, Tsukuba 305-0047, Japan*

The [Sm(Co,Cu)<sub>5</sub>/Fe]<sub>6</sub> multilayer film that was fabricated by annealing the Cr[a-SmCo<sub>6</sub>(9nm)/Cu(xnm)/Fe(5nm)/Cu(xnm)]<sub>6</sub>/Cr (x=0~0.75) multilayer has shown good in-plane texture and a high maximum energy product ( $BH$ )<sub>max</sub> of 32 MGOe with a coercivity of 7.24 kOe. The addition of the Cu layer between the a-SmCo<sub>6</sub> and Fe layers with optimum thickness increases the coercivity significantly, thereby improving the maximum energy product. The single-phase behavior and the irreversible rotation in the demagnetization process indicates strong exchange coupling between the Sm(Co,Cu)<sub>5</sub> and Fe layers.

PACS number: 75.50.Ww; 75.30.Et; 75.70.Cn

*Key words:* textured multilayer film, exchange coupling, maximum energy product,

The nanocomposite magnets that are composed of exchange coupled hard and soft magnetic phases have been a subject of recent studies for their potential to achieve the maximum energy product  $(BH)_{\max}$  that is higher than those achieved in the existing sintered magnets.<sup>1,2</sup> Although various types of nanocomposite magnets were reported in the Nd-Fe-B system, their coercivity ( $H_c$ ), remanence ( $B_r$ ), and  $(BH)_{\max}$  are lower than those for commercial sintered magnets of the same system due to their isotropic feature; thus, nanocomposite magnets are considered as economical medium performance materials for bonded magnet applications.<sup>3</sup> However, crystallographically textured anisotropic nanocomposites still have a great technological potential to achieve a higher  $(BH)_{\max}$ . Since many complicated metallurgical processes must be involved in producing anisotropic bulk nanocomposites, textured multilayer thin films will serve as a convenient model system for studying the fundamental properties of exchange-spring magnets.<sup>4,5</sup> The calculation by Skomski and Coey<sup>6</sup> predicted that the upper limit of  $(BH)_{\max}$  for anisotropic  $\text{Sm}_2\text{Fe}_{17}\text{N}_3/\text{Fe}_{65}\text{Co}_{35}$  multilayer with a volume fraction of only 9% of the hard phase was 137MGOe. Thus, an experimental demonstration of high  $(BH)_{\max}$  achievable by an anisotropic multilayer exchange spring magnet will boost the research toward new high performance permanent magnetic materials.

In this work, we selected  $\text{SmCo}_5$  with a huge  $K_u$  ( $K_u > 10^8$  erg/cc) as a hard phase and Fe as a soft phase. The previously reported textured multilayers were fabricated by depositing the Sm-Co and Fe or Co layers onto a heated substrate or by directly depositing the layers at room temperature,<sup>4,7</sup> and the reported  $(BH)_{\max}$  was only in the range of 10 to 20GMOe. In this paper, we report the good textured  $\text{Sm}(\text{Co,Cu})_5/\text{Fe}$  multilayer films fabricated by sputtering and subsequent annealing. After the

post-annealing, the multilayer structure was kept with a good in-plane c-axis texture. A high  $(BH)_{\max}$  of 32GMOe was obtained, which is larger than that achieved in the  $\text{SmCo}_5$  and  $\text{Sm}(\text{Co,Fe,Cu,Zr})_7$  type commercial sintered magnets.

The multilayer films were prepared by sequentially depositing Sm-Co, Cu, and Fe layers on a 100 nm thick Cr underlayer that was sputter deposited on a thermally oxidized Si wafer. The reason for adding the Cu interlayers is that it is immiscible with Fe, but can dissolve in the Sm-Co layer. The Sm-Co layers with a nominal composition of  $\text{SmCo}_6$  were deposited by co-sputtering Sm and Co targets. After depositing the multilayer films, a 50 nm thick Cr capping layer was deposited to protect the oxidation of the films. The structure of the Sm-Co layer was amorphous in the as-deposited condition, so the as-deposited films were  $\text{Cr}(50 \text{ nm})/[\text{a}-(\text{Sm-Co})(9 \text{ nm})/\text{Cu}(x \text{ nm})/\text{Fe}(5 \text{ nm})/\text{Cu}(x \text{ nm})]_6/\text{Cr}(100 \text{ nm})/\text{a-SiO}_2$ , where a- stands for amorphous. Then, the films were heat treated at temperatures ranging from 450°C to 525°C for 30min. The magnetic properties were measured using a superconducting quantum interference device (SQUID) magnetometer with a maximum magnetic field of 5.5 T. A preliminary examination of the film structure was made by x-ray diffraction (XRD) and the detailed microstructure was investigated by transmission electron microscopy (TEM).

Figure 1 shows the XRD results for the as-deposited  $\text{Cr}(50 \text{ nm})/[\text{a}-(\text{Sm-Co})(9 \text{ nm})/\text{Cu}(x \text{ nm})/\text{Fe}(5 \text{ nm})/\text{Cu}(x \text{ nm})]_6/\text{Cr}(100 \text{ nm})/\text{a-SiO}_2$  film and for the samples with different Cu thicknesses  $x=0$  and 0.5 annealed at 450°C for 30min. In the as-deposited state, the Sm-Co layer is amorphous. After annealing at 450°C for 30min, no clear peaks for a Sm-Co phase were detected in the Cu-free film ( $x=0$ ), suggesting that the Sm-Co layer is still amorphous. However, the film with  $x=0.5$  showed the

strong peaks corresponding to the  $\text{Sm}(\text{Co,Cu})_5$  hard phase ( $\text{CaCu}_5$ -type hexagonal structure), indicating that the addition of a Cu layer can reduce the crystallization temperature of the  $\alpha\text{-SmCo}_6$  layer and cause the hard layer to crystallize at the low temperatures.

The film with  $x=0.5$  shows an enhanced  $(11\bar{2}0)$  peak indicative of preferential in-plane texture of the c-axis. Figure 2 shows the in-plane and out-of-plane hysteresis loops of the film with  $x=0.5$  that was annealed at  $450^\circ\text{C}$  for 30 min. The film exhibits a strong in-plane anisotropy that is consistent with the XRD results. The in-plane hysteresis loop shows good squareness in the second quadrant, implying that this kind of film has the potential to be used as a permanent magnet. A coercivity  $H_c$  of 7.24 kOe and a maximum energy product  $(BH)_{\text{max}}$  of 32 MGOe were obtained in this film, which is larger than the  $(BH)_{\text{max}}$  values (20 – 28 MGOe) of the commercially available  $\text{SmCo}_5$  and  $\text{Sm}_2\text{Co}_{17}$ -type sintered permanent magnetic materials.

Table I shows  $H_c$ , remanence  $4\pi M_r$ , and  $(BH)_{\text{max}}$  of the multilayer films with different Cu thicknesses ( $x=0\sim 0.75$  nm) annealed at different temperatures for 30 min. For all of the as-deposited films, the annealing temperatures above  $450^\circ\text{C}$  led to the improvement of the coercivities, while the remanences decreased slightly. With the increase of Cu thickness, the coercivities increased significantly, especially at the low annealing temperature of  $450^\circ\text{C}$ . However, the coercivity decreased with  $x=0.75$  nm. Due to the improvement of coercivity,  $(BH)_{\text{max}}$  increases after the addition of the Cu layer.

Figure 3 shows the TEM bright field image of the multilayer film with  $x=0.5$  annealed at  $500^\circ\text{C}$  for 30 min. The multilayer structure remains in the film after annealing. The multilayer is composed of  $\text{Sm}(\text{Co,Cu})_5$  and Fe layers, and does not

have any Cu layers remaining. This is because the Cu-layer and the a-Sm-Co layer interdiffused and became a  $\text{Sm}(\text{Co,Cu})_5$  phase. The elemental distribution in the multilayer structure was examined by the energy filtered elemental map as shown in Fig. 4. The soft layer (Fe layer) and the hard layer (Sm layer) are clearly observed. Cu is partitioned in the  $\text{Sm}(\text{Co,Cu})_5$  layer without being dissolved in the Fe layer, which is evident from the intensity profile of the elements as shown in Fig. 4. The intensity profile shows that the Co layer becomes wider in comparison with the thickness of the Sm layer, indicating that some amount of Co atoms diffuse from the hard layer into the Fe layer to form FeCo solid solution near the interface. This is because the a-SmCo<sub>6</sub> phase contained excess amount of Co for the formation of the SmCo<sub>5</sub> phase.

The films contain a large amount of Fe soft phase (higher than 33vol%); however, the shape of the hysteresis loop is of a single hard magnetic phase with a distinctive squareness compared with that of the previously reported films<sup>4,8</sup> (see Fig. 1). Two reasons are thought to be responsible for this squareness. The first is the presence of aligned hard layers. Another is the extremely strong exchange coupling between the hard and soft layers which causes the two layers to switch together. According to the exchange spring model of Kneller and Hawig,<sup>9</sup> the soft layer has a critical thickness  $t_{cs} = 2\pi\sqrt{A_s/2K_k}$ , where  $A_s$  is the exchange energy of the soft phase and  $K_k$  is the magnetocrystalline anisotropy constant of the hard phase. If the thickness of the soft layer,  $t_s$ , is  $t_s \leq t_{cs}$ , the hard and soft layers will switch simultaneously and the demagnetization curve will show a single-phase behavior. If  $t_s \gg t_{cs}$ , the demagnetization curve with hard and soft components will appear. For the SmCo<sub>5</sub> hard phase, the critical thickness of the Fe layer is about 5.4 nm ( $A_s = 2.5 \times 10^{-11} \text{ J/m}$  and  $K_k = 1.71 \times 10^7 \text{ J/m}^3$ )<sup>10</sup>. The thickness of the Fe layer in our films is about 5 nm,

which is very close to the critical thickness. This means that the entire volume of the soft layers is strongly coupled with the hard layers in the films and that the two layers switch as a single hard layer. This is consistent with our experimental result.

To gain further insight into the demagnetization process, we measured the recoil curve of the film with  $x=0.5$  annealed at  $450^{\circ}\text{C}$  for 30min as shown in Fig. 5 (a). The recoil curve looks different from that of the melt spun nanocomposite magnet (open recoil curve), and is similar to that of the single-phase magnet prepared by melt-spinning,<sup>11</sup> although the film contains a large amount of soft phase (higher than 33.3vol%). This may be due to the nanosized homogeneous microstructure in the film, so that the entire volume of the soft phase is strongly coupled with the hard phase. The irreversible rotation of the magnetic moment can be quantitatively analyzed by plotting the irreversible change in magnetization –  $M_{\text{irrev}}(H)/2M_r = [M_r - M_d(H)]/2M_r$  vs the reverse field  $H$  (see Fig. 5 (b)), where  $M_r$  is the saturation remanence and  $M_d(H)$  is the field-demagnetization remanence obtained from the recoil curve.<sup>11</sup> From this plot, we can obtain the nucleation field  $H_n$  for irreversible rotation of the hard layer with a value of about 7 kOe. –  $M_{\text{irrev}}(H)/2M_r$  is around zero until  $H_n$ , where it increases very rapidly. The change in  $H_n$  is very sharp, suggesting that most of the hard layers switch together with the soft phase in the field  $H_n$ . In the fields less than  $H_n$ , –  $M_{\text{irrev}}(H)/2M_r$  is almost zero, implying that the irreversible rotation of the soft layers does not occur in the fields below  $H_n$ . This indicates that the soft layers are totally coupled with the hard layers.

Compared to the Cu-free film, the films with Cu  $x=0.3$  and  $0.5$  exhibit a large coercivity, especially at the annealing temperature of  $450^{\circ}\text{C}$  (see Table I). The XRD data (see Fig.1) shows that the Sm-Co layer of the Cu-free film is still amorphous at

the annealing temperature of 450°C. However, the hard layer can crystallize into a hard  $\text{Sm}(\text{Co,Cu})_5$  phase at 450°C after the addition of the Cu layers. So the coercivity of Cu-containing films increases significantly. At the annealing temperatures of 500°C and 525°C, the coercivities of the films with  $x=0.3$  and  $0.5$  are still larger than that of the Cu-free films. We assume that this can also be attributed to the  $\text{Sm}(\text{Co,Cu})_5$  phase which shows a reduced crystallization temperature due to the addition of Cu. A larger amount of Fe will diffuse into the  $\text{SmCo}_5$  layer to form the  $\text{Sm}-(\text{Co,Fe})$  phase unless there is a Cu layer between the a-Sm-Co and Fe layers. This would decrease the magnetocrystalline anisotropy of the Sm-Co phase significantly, which would result in a lower coercivity. Cu will only diffuse into the a-Sm-Co layer, because Cu cannot dissolve in the Fe phase. Although Cu also decreases the anisotropy of the  $\text{Sm}(\text{Co,Cu})_5$  phase, some amount of replacement of Cu with Co was reported not to decrease the anisotropy largely or even to increase the anisotropy.<sup>12</sup> This assumption needs further investigation. Furthermore, only a large amount of Fe and Cu can decrease the anisotropy of Sm-Co phase significantly. This may be the reason for the rapid decrease of coercivity in films with  $x=0.75$ .

In summary, we have successfully fabricated the exchange coupled  $[\text{Sm}(\text{Co,Cu})_5/\text{Fe}]_6$  multilayer films that approach the ideal exchange-spring magnets with aligned hard and soft layers by post-annealing the  $\text{Cr}(50 \text{ nm})/[\text{a}-(\text{Sm-Co}) (9 \text{ nm})/\text{Cu} (x \text{ nm})/\text{Fe} (5 \text{ nm})/\text{Cu} (x \text{ nm})]_6/\text{Cr} (100 \text{ nm})/\text{a-SiO}_2$  multilayers. The addition of a Cu interlayer between the a-Sm-Co and Fe layers with an appropriate thickness improved the coercivity and  $(BH)_{\text{max}}$ , especially at the low annealing temperatures. This is related to the reduced crystallization temperature of the amorphous Sm-Co phase as well as the substitution of Cu for Co to form the  $\text{Sm}(\text{Co,Cu})_5$  phase. The

largest  $(BH)_{\max}$  was 32 MGOe, which is larger than the theoretical limit for a  $\text{SmCo}_5$  single phase magnet, 28.8 MGOe. This value is also larger than those of the commercial  $\text{SmCo}_5$  and  $\text{Sm}(\text{Co,Fe,Cu,Zr})_7$  type sintered magnets. By replacing Fe with  $\text{Fe}_{65}\text{Co}_{35}$  or adjusting the thickness of hard and soft layers, it will be possible to enhance the  $(BH)_{\max}$  further. This work has demonstrated that there is a potential to develop high performance exchange spring magnets by optimizing nanocomposite microstructures.

### **Acknowledgement**

This work was supported partly by the Special Coordination Funds for Promoting Science and Technology on “Nanohetero Metallic Materials” from the Ministry of Education, Culture, Sports, Science and Technology. JZ and YKT acknowledge the Japan Science Promotion Society for the JSPS fellowships. The authors thank Dr. T. O. Seki for her help in sample preparation and magnetic measurements and Dr. C. Y. You for the helpful discussions.

## References

- <sup>1</sup> R. Skomski and J. M. D. Coey, Phys. Rev. B **48**, 15812 (1993).
- <sup>2</sup> D. J. Sellmyer, Nature **420**, 374 (2002).
- <sup>3</sup> V. Archambault, and D. Pere, Mat. Res. Soc. Symp. Pro., **577**, 153 (1999)
- <sup>4</sup> E. E. Fullerton, J. S. Jiang, C. H. Sowers, J. E. Pearson, and S. D. Bader, Appl. Phys. Lett. **72**, 380 (1998); E. E. Fullerton, J. S. Jiang, M. Grimsditch, C. H. Sowers, and S. D. Bader, Phys. Rev. B **58**, 12193 (1998).
- <sup>5</sup> R. Röhlsberger, H. Thomas, K. Schlage, E. Burkel, O. Leupold, and R. Rüffer, Phys. Rev. Lett. **89**, 237201 (2002); V. K. Vlasko-Vlasov, U. Welp, J. S. Jiang, D. J. Miller, G. W. Crabtree, and S. D. Bader, Phys. Rev. Lett. **86**, 4386 (2001).
- <sup>6</sup> R. Skomski and J. M. D. Coey, Phys. Rev. B **48**, 15812 (1993).
- <sup>7</sup> I. A. Al-Omari and D. J. Sellmyer, Phys. Rev. B **52**, 3441 (1995).
- <sup>8</sup> W. Liu, Z. D. Zhang, J. P. Liu, L. J. Chen, L. L. He, Y. Liu, X. K. Sun, and D. J. Sellmyer, Adv. Mater. **14**, 1832 (2002).
- <sup>9</sup> E. F. Kneller, and R. Hawig, IEEE Trans. Magn. **27**, 3588 (1991).
- <sup>10</sup> T. Schrefl, R. Fischer, J. Fidler, and H. Kronmüller, J. Appl. Phys. **76**, 7053 (1994).
- <sup>11</sup> D. Goll, M. Seeger, and H. Kronmüller, J. Magn. Magn. Mater. **185**, 49 (1998).
- <sup>12</sup> E. Lectard, C. H. Allibert, and R. Ballou, J. Appl. Phys. **75**, 6277 (1994).

## Table caption

Table I The coercivity  $H_c$ , remanence  $4\pi M_r$ , and maximum energy product  $(BH)_{\max}$  of Cr(50 nm)/[a-(Sm-Co)(9nm)/Cu(xnm)/Fe(5nm)/Cu(xnm)]<sub>6</sub>/Cr(100 nm)/a-SiO<sub>2</sub> films with different Cu thicknesses ( $x=0\sim 0.75$ nm) annealed at different temperatures for 30min.

## Figure captions

Fig. 1 The XRD results for the as-deposited film and the Cr(50 nm)/[a-(Sm-Co)(9nm)/Cu(xnm)/Fe(5nm)/Cu(xnm)]<sub>6</sub>/Cr(100nm)/a-SiO<sub>2</sub> films with different Cu thicknesses  $x=0$  and 0.5 annealed at 450°C for 30min;

Fig. 2 The in-plane and out-of-plane hysteresis loops of the film with  $x=0.5$  annealed at 450°C for 30min.

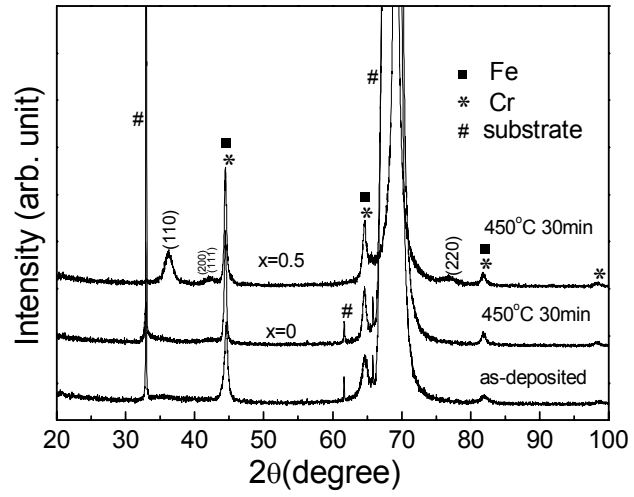
Fig. 3 The TEM bright field image of the film with  $x=0.5$  annealed at 500°C for 30min.

Fig. 4 Electron energy loss spectroscopy (EELS) maps of Sm, Co, Fe, and Cu of the film with  $x=0.5$  annealed at 500°C for 30min and the intensity profile of the elements obtained from the EELS maps.

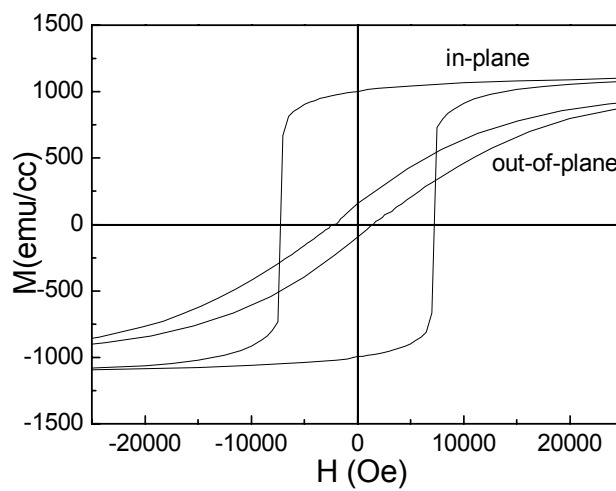
Fig. 5 The recoil curve (a) and dependence –  $M_{\text{irrev}}(H)/2M_r$  on the reverse field  $H$  (b) for the film with  $x=0.5$  annealed at 450°C for 30min.

Table I The coercivity  $H_c$ , remanence  $4\pi M_r$ , and maximum energy product  $(BH)_{\max}$  of the Cr(50nm)/[a-(Sm-Co)(9nm)/Cu(xnm)/Fe(5nm)/Cu(xnm)]<sub>6</sub>/Cr(100nm)/a-SiO<sub>2</sub> films with different Cu thicknesses ( $x=0\sim 0.75$ nm) annealed at different temperatures for 30min.

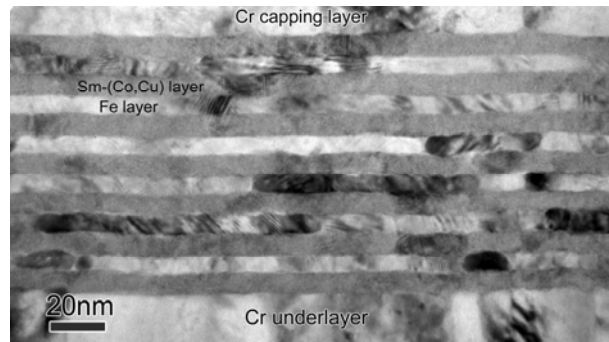
Composition	Annealing conditions	$H_c$ (kOe)	$4\pi M_r$ (kGs)	$(BH)_{\max}$ (MGOe)
X=0	450°C 30min	1.22	13.2	9
	500°C 30min	6.25	12.2	29
	525°C 30min	6.24	12.1	27
X=0.3	450°C 30min	6.74	12.6	31
	500°C 30min	7.26	12.4	31
	525°C 30min	7.48	12.1	30
X=0.5	450°C 30min	7.24	12.6	32
	500°C 30min	8.25	12.2	30
	525°C 30min	8.26	12.3	31
X=0.75	450°C 30min	5.28	12.7	31
	500°C 30min	5.91	12.3	30
	525°C 30min	6.26	11.8	27



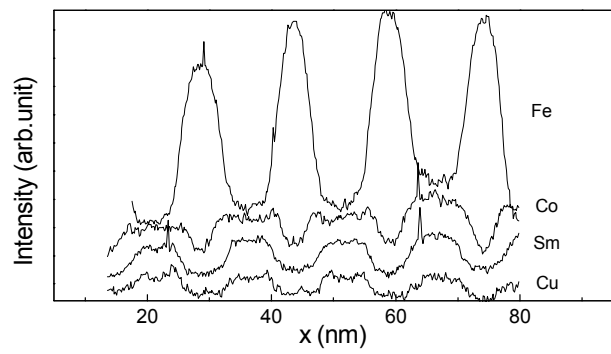
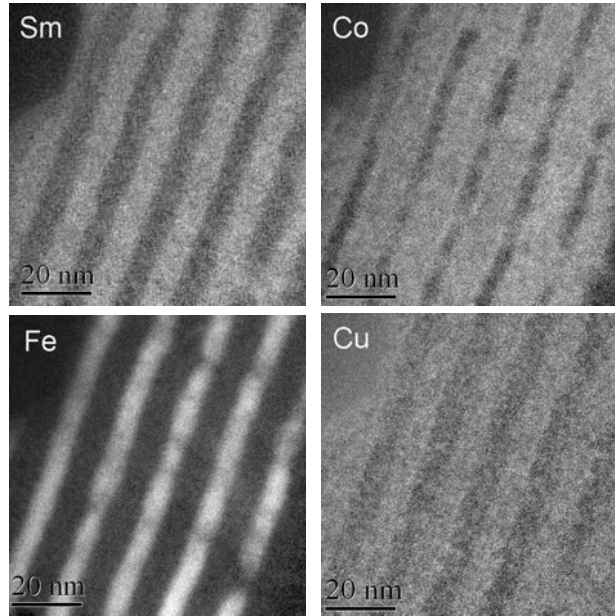
Jian Zhang *et al.* Fig. 1



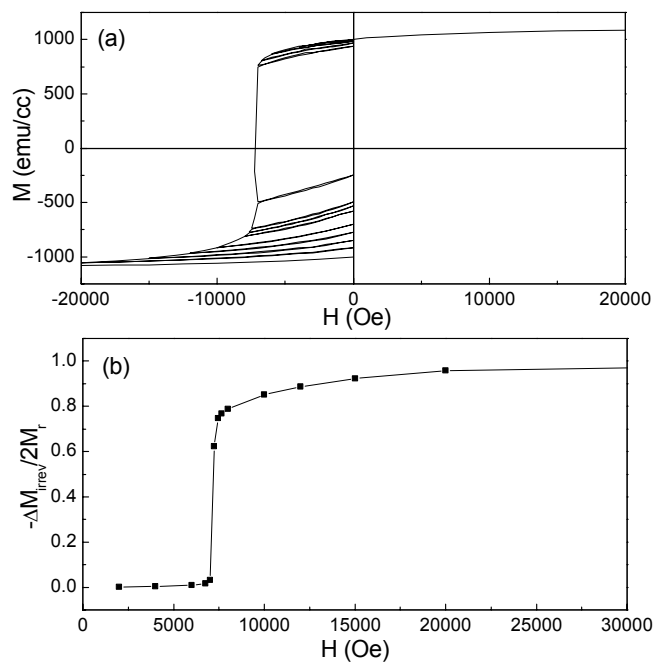
Jian Zhang *et al.* Fig. 2



Jian Zhang *et al.* Fig. 3



Jian Zhang *et al.* Fig. 4



Jian Zhang *et al.* Fig. 5